

## Mechanical, Hygric, and Thermal Properties of Cement-Based Composite with Hybrid Fiber Reinforcement Subjected to High Temperatures

Eva Vejmelková · Petr Konvalinka ·  
Pavel Padevět · Lubomír Kopecký ·  
Martin Keppert · Robert Černý

Received: 10 September 2008 / Accepted: 9 June 2009 / Published online: 23 June 2009  
© Springer Science+Business Media, LLC 2009

**Abstract** The tensile strength, bending strength, water vapor diffusion resistance factor, gas permeability, thermal conductivity, specific heat capacity, and linear thermal expansion coefficient of a cement-based composite with hybrid PVA-fiber reinforcement are determined as functions of thermal pre-treatment, the loading temperatures being 600 °C, 800 °C, and 1000 °C. The experimental results show that the most important changes in all studied parameters occur between the unloaded state and the loading temperature of 600 °C and then between 800 °C and 1000 °C. Although seemingly high, these changes are still small as compared to many other cement-based composites. The positive effect of using PVA fibers for the high-temperature behavior of the studied composite can be seen mainly in their ability to prevent thermal spalling which is a serious deterioration effect for cement-based composites.

**Keywords** Cement-based composites · Hybrid fiber reinforcement · Hygric properties · Mechanical properties · Thermal load · Thermal properties

---

E. Vejmelková · M. Keppert · R. Černý (✉)  
Department of Materials Engineering and Chemistry, Faculty of Civil Engineering,  
Czech Technical University in Prague, Thákurova 7, Prague 6 166 29, Czech Republic  
e-mail: cernyr@fsv.cvut.cz

P. Konvalinka  
Experimental Center, Faculty of Civil Engineering, Czech Technical University in Prague,  
Thákurova 7, Prague 6 166 29, Czech Republic

P. Padevět · L. Kopecký  
Department of Mechanics, Faculty of Civil Engineering, Czech Technical University in Prague,  
Thákurova 7, Prague 6 166 29, Czech Republic

## 1 Introduction

Cementitious composites reinforced by short, randomly distributed fibers began to gain in importance in the concrete industry since the 1960s. The benefits of fiber reinforcement in improving the fracture toughness, impact resistance, fatigue endurance, and energy absorption capacity of concrete were quite clear arguments for their increasing use. In the 1980s the fiber reinforcement gradually moved up towards multifunctionality, and hybrid-fiber reinforcement appeared in cement-based composites. The attractive advantages of hybrid fiber systems were seen in the convenient combination of their mechanical performance. Three basic hybrid fiber arrangements were devised [1]. In the first, the stronger and stiffer fiber improved the first crack stress and ultimate strength, and the flexible and ductile fiber improved the toughness and strain capacity in the post-cracking zone. The second hybrid fiber system consisted in using combination of smaller fibers, which bridged microcracks and controlled their growth, thus increasing the tensile strength of the composite, and larger fibers which could arrest the propagating macrocracks, thus substantially improving the toughness of the composite. In the third hybrid fiber arrangement, the durability of fiber types was different. The presence of the durable fiber increased the strength and/or toughness retention after age while another type was to guarantee the short-term performance during transportation and installation of the composite elements.

The basic arguments for using hybrid-fiber reinforced cement composites formulated in [1] remained topical hitherto, but research activities on this composite type were not very extensive since their first appearance. The rare occurrence of references to this topic found in the scientific literature (only several tens in Web of Science (WoS) during the last 20 years) underlines well this statement. The experimental studies performed by Qian and Stroeven [2] for the combination of steel and polypropylene fibers in cement matrix, Sun et al. [3] for steel, PVA, and polypropylene fibers, Ahmed et al. [4] for steel and polyethylene fibers, Sahmaran and Yaman [5] for two types of steel fibers, and Sivakumar and Santhanam [6] for steel and various non-metallic fibers (polypropylene, polyester and glass) belong to the few exceptions in this respect. Therefore, investigations of the proper preparation procedures and properties of hybrid-fiber reinforced cement composites still present an actual research problem.

During the last two decades, fire safety considerations appeared as the additional sound argument for using hybrid fibers. With the increasing use of high-performance concrete having very low porosity, thus very limited capability of water and water vapor transport, in the building industry, the risk of explosive spalling in concrete elements at high temperatures became apparent. Incorporation of fibers with high melting points, which were responsible for the strength and/or toughness retention, and fibers with low melting points, which evaporated after high-temperature exposure and provided passages for water vapor to escape, presented a promising solution to enhance concrete resistance to spalling. For instance, a combination of steel and polypropylene fibers was found to be an effective solution in this respect by several researchers [7–9].

In this study, the effect of application of two different types of PVA fibers on the mechanical, thermal, and hygric properties of a cementitious composite is investigated. The parameters of the composite are analyzed in both the reference state and

**Table 1** Composition of the studied composite material in mass%

Component	Quantity
Cement CEM I 52.5	54.0
Siliceous aggregates	27.0
Microdorsillite 405	13.0
Microsilica 940 US	3.0
Kuralon RECS 100/12 mm	1.5
Kuralon RECS 7/6 mm	0.5
Glenium ACE 40	1.0

after pre-heating up to 1000 °C. Therefore, its performance can be assessed in both common service conditions on a building site and under conditions of a fire.

## 2 Technology of Sample Preparation

The composition of the analyzed hybrid PVA-fiber reinforced cement composite is shown in Table 1. Water in the amount corresponding to the w/c ratio of 0.32 was added to the mixture.

Samples for measurements were prepared in the laboratories of Vustah Brno using an Omni Mixer 10 EV vacuum mixing device. At first, cement, siliceous aggregates, microsilica, and microdorsillite were homogenized in the mixing device; then water, plasticizer, and shorter PVA fibers were added and the wet mixture mixed again. Finally, the longer PVA fibers were stirred into the mixture. The liquid mixture was cast into forms and de-aerated during 1 h. After a time period of 28 days after mixing, the samples were prepared for testing.

In the experimental measurements, four different sample pre-treatment conditions were tested:

- reference specimens not exposed to any load (denoted as K-ref in what follows)
- specimens exposed to a gradual temperature increase up to (600 °C, 800 °C and 1000 °C) for 2 h, then left for next 2 h at the final temperature, and slowly cooled (denoted as K-600, K-800, and K-1000 according to the loading temperature).

For every pre-treatment, three specimens were used for testing. Before the measurements of all parameters, specimens were dried in an oven at 110 °C.

## 3 Experimental Methods

The basic characterization of the changes of internal structure and composition due to high-temperature exposure was carried out using the XL30 ESEM-TMP device with an EDAX microanalyzer. Main attention was paid to the interfacial transition zone between the PVA fibers and the cement paste. The methodology of the analysis was based on the profile measurements between the fiber and cement paste.

The basic physical properties were studied using the water vacuum saturation method [10], helium pycnometry, and mercury porosimetry. The bulk density  $\rho$  ( $\text{kg} \cdot \text{m}^{-3}$ ), total open porosity  $\psi$  ( $\% \text{m}^3/\text{m}^3$ ), matrix density  $\rho_{\text{mat}}$  ( $\text{kg} \cdot \text{m}^{-3}$ ), and median pore diameter were the analyzed parameters. The samples used for determination of basic properties by the water vacuum saturation method were cut from the standard prisms; their sizes were  $40 \text{ mm} \times 40 \text{ mm} \times 20 \text{ mm}$ . Mercury porosimetry was done using Thermo Pascal 140 and 440 devices; the mass of the specimens was approximately 1 g. For the helium pycnometry measurements, Porotec Pycnomatic ATC equipment was used; the mass of the specimens was approximately 15 g.

The measurement of the tensile strength was done by an electromechanical testing device MTS Alliance RT 30 with a maximum tension force of 30 kN. The rate of loading was  $0.025 \text{ mm} \cdot \text{min}^{-1}$ ; the dimensions of the specimens were  $20 \text{ mm} \times 10 \text{ mm} \times 160 \text{ mm}$ . The bending strength was measured in the same device provided with a three-point bending track 642.01 A which allows a maximum load of 27.80 kN. The rate of loading was  $0.04 \text{ mm} \cdot \text{min}^{-1}$ , the dimensions of the specimens were  $40 \text{ mm} \times 40 \text{ mm} \times 160 \text{ mm}$ .

The wet-cup and dry-cup methods were employed in the measurements of water vapor transport parameters [10]. The water vapor permeability  $\delta$  (s), water vapor diffusion coefficient  $D$  ( $\text{m}^2 \cdot \text{s}^{-1}$ ), and water vapor diffusion resistance factor  $\mu$  (–) were determined. Using the measured data for the dry-cup water vapor permeability, the values of the material gas permeability ( $\text{m}^2$ ) were calculated. The samples for measurement of water vapor transport properties were cylinders with a diameter of 120 mm and a length of 20 mm and were water- and water vapor-proof insulated with epoxy resin on the lateral sides to ensure one-dimensional transport.

The thermal conductivity  $\lambda$  ( $\text{W} \cdot \text{m}^{-1} \cdot \text{K}^{-1}$ ) and specific heat capacity  $c$  ( $\text{J} \cdot \text{kg}^{-1} \cdot \text{K}^{-1}$ ) were measured using the commercial device Isomet 2104 (Applied Precision, Ltd). The measurement was based on the analysis of the temperature response of the analyzed material to heat flow impulses. The samples for determination of thermal properties had a size of  $70 \text{ mm} \times 70 \text{ mm} \times 70 \text{ mm}$ . The linear thermal expansion coefficient was measured using a comparative method [11]. The dimensions of the specimens were  $40 \text{ mm} \times 40 \text{ mm} \times 120 \text{ mm}$ .

#### 4 Experimental Results and Discussion

Figure 1 shows that in the reference material not subjected to any thermal load the adhesion of cement paste and the fiber was very good. A very small number of pores appeared in the interfacial transition zone (ITZ) between the fiber and the cement paste; the contact was very tight all along the fiber. Low  $\text{Ca}^{2+}$ -ion saturated C–S–H gels, ettringite, and portlandite were found up to a distance of  $15 \mu\text{m}$  from the fiber. In the interval of  $15 \mu\text{m}$  to  $30 \mu\text{m}$  from the fiber, the  $\text{Ca}^{2+}$ -ion saturation increased, and  $\text{C}_2$ –S–H gels appeared at the expense of ettringite and portlandite. A fully Ca-saturated ( $\text{C}_3$ –S–H) gel was observed approximately  $30 \mu\text{m}$  from the fiber.

After  $600^\circ\text{C}$  pre-heating, the PVA fibers were completely disintegrated (a trace in the matrix where originally a fiber was is well visible in Fig. 2); after the decomposition and oxidation of PVA, just carbon residue remained. The ITZ-layer lost the water

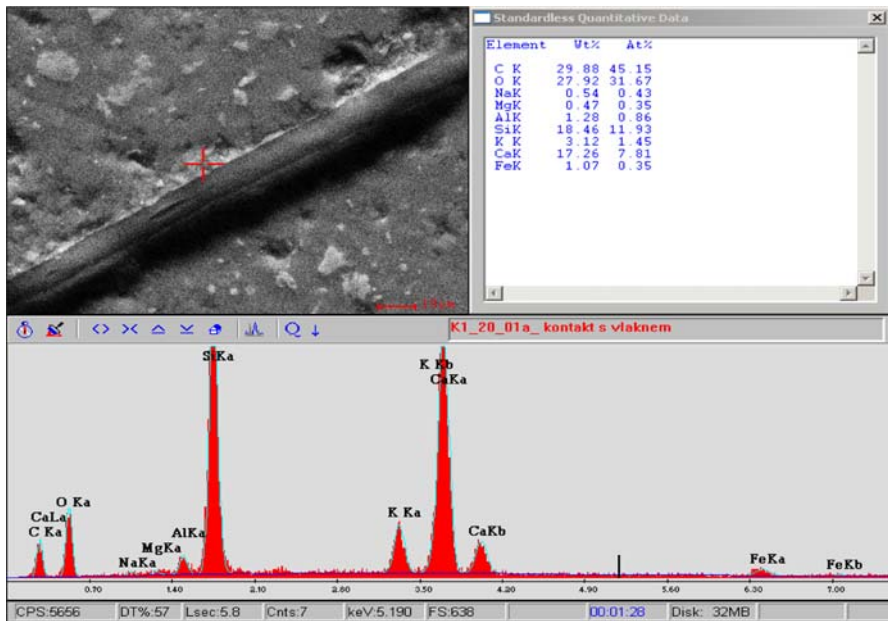


Fig. 1 Microstructural analysis—reference specimen

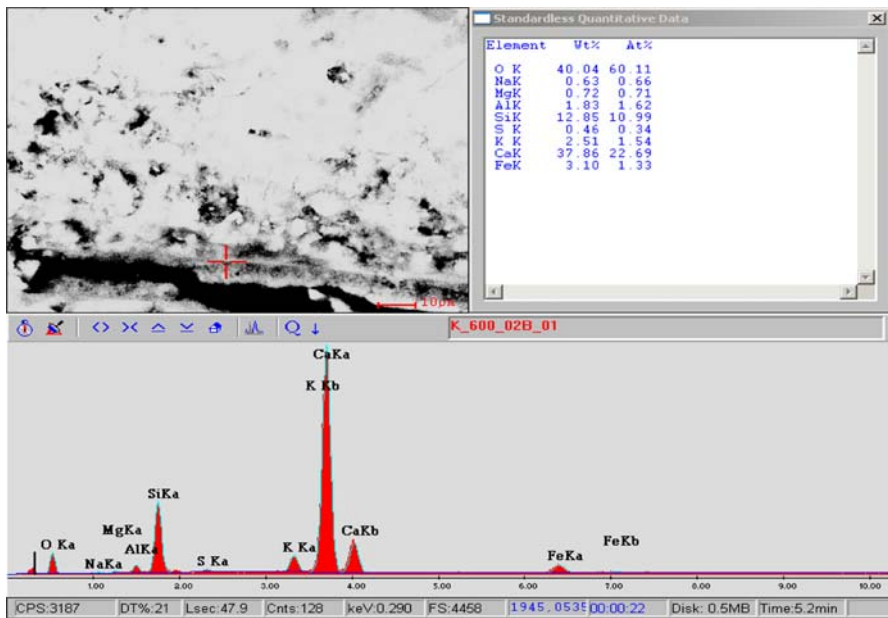
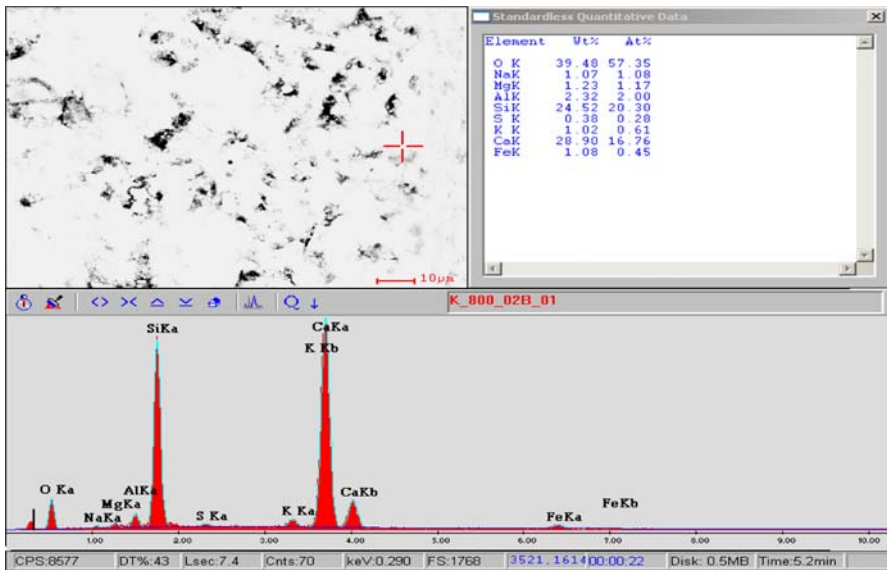


Fig. 2 Microstructural analysis—specimen pre-heated to 600 °C



**Fig. 3** Microstructural analysis—specimen pre-heated to 800 °C

chemically bound in portlandite and C–S–H gels. This led to the decomposition of both portlandite and a substantial part of C–S–H gels and to the appearance of CaO and wollastonite in the zone adjacent to the fiber; at a larger distance from the fiber a small amount of mullite (sillimanite) was also found. The damage of the cement matrix in the vicinity of the fiber was not yet very serious. Clearly, the early disintegration of PVA fibers prevented the matrix effectively from explosive spalling.

Figures 3 and 4 present the results of microstructural analysis of specimens pre-heated to 800 °C and 1000 °C. Apparently, the level of deterioration of the original cement hydration products was higher than for the 600 °C pre-heated specimen. The C–S–H gels were, after loss of all water, partially transformed to calcium-silicate minerals similar to  $C_2S$  and  $C_3S$ ; a substantial part of the original C–S–H gels was completely thermally decomposed, and CaO and  $SiO_2$  appeared. These parts of the specimens had a very low internal cohesion and were crushed during the surface preparation.

Table 2 shows basic parameters of the studied material depending on the loading temperature which were measured by the water vacuum saturation method. The most important change in porosity occurred between the unloaded state and the loading temperature of 600 °C where the increase of porosity was as high as 54 %. Subsequent porosity changes were less than 10 %.

The helium pycnometry measurements in Table 3 showed 10 % to 20 % lower open porosity than water vacuum saturation experiments in Table 2 for the reference material and the material pre-heated to 600 °C. These differences were probably caused by residual cement hydration under conditions of water vacuum saturation which increased the matrix density. For higher pre-heating temperatures, the agreement of both methods was very good.

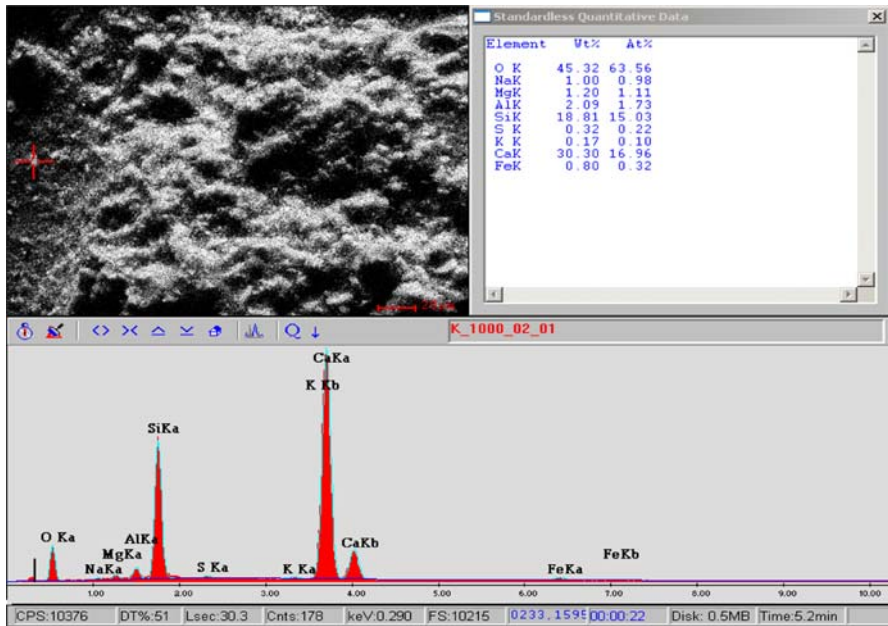


**Fig. 4** Microstructural analysis—specimen pre-heated to 1000 °C

**Table 2** Basic properties of the studied composite material measured by the water vacuum saturation method

Material	$\rho$ ( $\text{kg} \cdot \text{m}^{-3}$ )	$\rho_{\text{mat}}$ ( $\text{kg} \cdot \text{m}^{-3}$ )	$\psi$ ( $\% \text{m}^3/\text{m}^3$ )
K-ref	2030	2590	21.6
K-600	1940	2910	33.2
K-800	1880	2900	35.1
K-1000	1840	2910	36.7

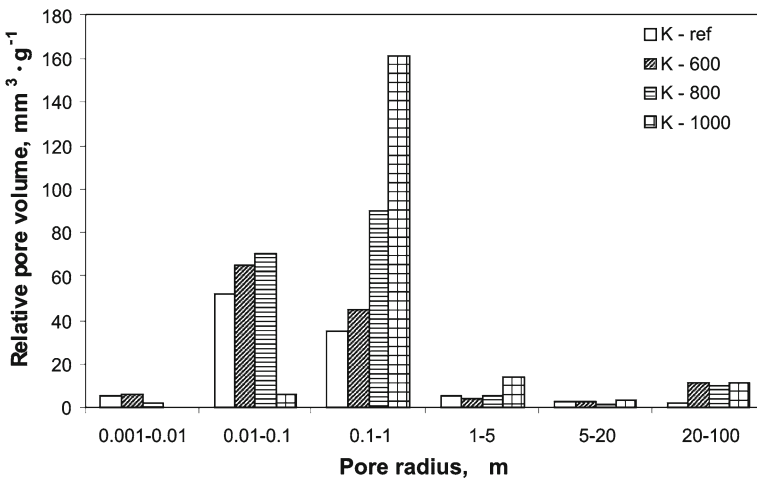
**Table 3** Basic properties of the studied composite material measured by helium pycnometry

Material	$\rho_{\text{mat}}$ ( $\text{kg} \cdot \text{m}^{-3}$ )	$\psi$ ( $\% \text{m}^3/\text{m}^3$ )
K-ref	2460	17.5
K-600	2730	29.0
K-800	2920	35.6
K-1000	2940	37.4

The total porosity measured by mercury porosimetry (Table 4) agreed very well with the data obtained by the water vacuum saturation method and helium pycnometry only for the specimens pre-heated to 800 °C and 1000 °C. For the reference specimens the porosity was very close to the water vacuum saturation measurement, thus about 20 % higher than in helium pycnometry. For 600 °C pre-heating, it was about 10 % lower compared to the helium pycnometry data. These results probably reflected the size effect; the specimens used in mercury porosimetry were much smaller than in the other two methods.

**Table 4** Basic properties of the studied composite material measured by mercury porosimetry

Material	Pore volume ( $\text{cm}^3 \cdot \text{g}^{-1}$ )	Pore surface area ( $\text{m}^2 \cdot \text{g}^{-1}$ )	Median pore diameter ( $\mu\text{m}$ )	Bulk density ( $\text{kg} \cdot \text{m}^{-3}$ )	Porosity ( $\% \text{m}^3/\text{m}^3$ )
K-ref	0.101	5.0	0.088	2100	21.2
K-600	0.133	5.8	0.090	2000	26.6
K-800	0.179	5.2	0.125	2000	35.8
K-1000	0.196	1.4	0.396	1900	37.2

**Fig. 5** Pore size distribution of the studied composite material

The pore volume increased by about 30 % between the reference state and 600 °C pre-heating, and this increase was accompanied by an approximately 15 % increase of pore surface area. The median pore diameter was changed only slightly. The measurement of pore size distribution (Fig. 5) showed that the differences were most important in the range of 20  $\mu\text{m}$  to 100  $\mu\text{m}$ . This was mainly due to the thermal decomposition of PVA fibers resulting in an appearance of their traces in the matrix (Fig. 2). The smaller pores were apparently not destructed in a very significant way. The PVA fibers played here a positive role acting as channels for removal of gases produced in thermal decomposition processes. This is in very good agreement with the ESEM material characterization experiments described before (Figs. 1, 2). Between the 600 °C and 800 °C pre-heating temperatures, a similar effect was observed. An approximately 30 % increase in pore volume was measured, with only 10 % decrease in pore surface area and about 40 % increase of median pore diameter. The most important changes in pore size distribution (Fig. 5) appeared between 800 °C and 1000 °C. While the number of pores in the range of 0.1  $\mu\text{m}$  to 1  $\mu\text{m}$  increased several times, the number of smaller pores decreased. This adds new information to the ESEM material characterization data which for these pre-heating temperatures (Figs. 3, 4) were less

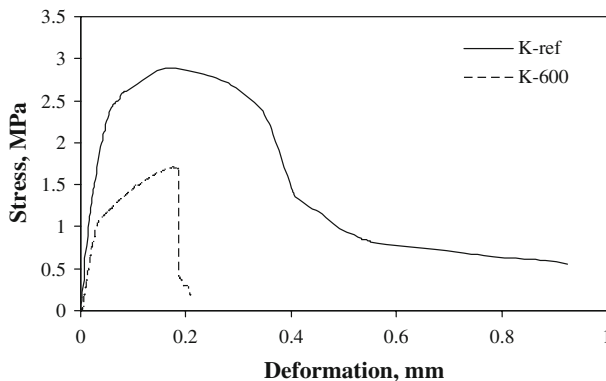
**Table 5** Deformation at failure and tensile strength of the studied composite material

Material	Deformation (mm)	Tensile strength (MPa)
K-ref	0.198	3.38
K-600	0.214	2.11

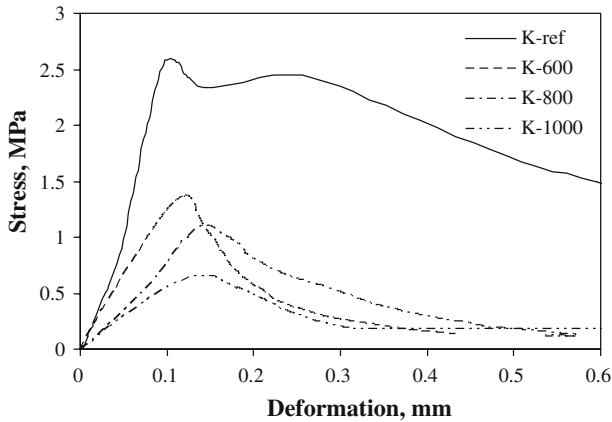
distinct than for the reference specimens and 600 °C pre-heating. The damage of the material structure was much more severe for 1000 °C pre-heating than for 800 °C.

Table 5 shows that significant differences in tensile strength were observed between the specimens in the reference state and those loaded to 600 °C. The decrease in tensile strength was almost 40%. Figure 6 shows a characteristic example of the stress–deformation curves in tension. The loss of fibers after heating to 600 °C was a rather important factor leading to an abrupt material failure which is commonly observed for regular concrete without fiber reinforcement. The specimens loaded to 800 °C and 1000 °C could not be investigated because their fixing into the testing device could not be done in a proper way due to considerable thermal deterioration.

The most important changes in bending strength (Table 6) and stress–deformation curves in bending (Fig. 7) were observed between the reference state and the specimens pre-heated to 600 °C where a 50% decrease of bending strength and rather different stress–deformation behavior were found. The changes in bending parameters between the specimens loaded to 800 °C and 1000 °C were also significant; another 50% decrease in bending strength was observed. This was in very good agreement with both ESEM analyses and mercury porosimetry data. The first loss of strength was

**Fig. 6** Stress–deformation curve in tension of the studied composite material**Table 6** Deformation at failure and bending strength of the studied composite material

Material	Deformation (mm)	Bending strength (MPa)
K-ref	0.095	2.50
K-600	0.134	1.25
K-800	0.143	1.19
K-1000	0.148	0.57



**Fig. 7** Stress–deformation curve in bending of the studied composite material

**Table 7** Water vapor transport properties of the studied composite material

Material	5/25–30 %			97/25–30 %		
	$\delta$ (s)	$D$ ( $\text{m}^2 \cdot \text{s}^{-1}$ )	$\mu$ (–)	$\delta$ (s)	$D$ ( $\text{m}^2 \cdot \text{s}^{-1}$ )	$\mu$ (–)
K-ref	$2.1 \times 10^{-12}$	$2.9 \times 10^{-7}$	79	$3.3 \times 10^{-12}$	$4.6 \times 10^{-7}$	51
K-600	$6.2 \times 10^{-12}$	$8.6 \times 10^{-7}$	27	$6.7 \times 10^{-12}$	$9.2 \times 10^{-7}$	25
K-800	$1.0 \times 10^{-11}$	$1.4 \times 10^{-6}$	16	$1.6 \times 10^{-11}$	$2.2 \times 10^{-6}$	10
K-1000	$1.2 \times 10^{-11}$	$1.7 \times 10^{-6}$	13	$2.1 \times 10^{-11}$	$2.8 \times 10^{-6}$	8

mainly due to the loss of fibers, the second due to the matrix deterioration processes in the high-temperature range.

The water vapor transport parameters of the studied material are shown in Table 7. We can see that the values of the water vapor diffusion resistance factor decreased very rapidly with the increasing load temperature for both configurations of the cup experiment. The most important was the change between the unloaded state and the loading temperature of 600 °C. This is in basic agreement with both the porosity and mechanical parameters data. The water vapor diffusion resistance factor for the wet-cup arrangement was significantly lower than for the dry-cup measurement. This concurs with the measurements obtained for many other building materials and reflects the partial inclusion of liquid water transport into the water vapor transport coefficient in the wet-cup experiment [12].

The values of gas permeability which are given in Table 8 increased in the most remarkable way between the reference state and the pre-heating temperature of 600 °C. This is in qualitative agreement with the changes of mechanical parameters.

Table 9 shows that after high-temperature loading the thermal conductivity in the dry state significantly decreased. This is in qualitative agreement with the increase of porosity due to decomposition reactions in the high-temperature range leading to an increase of significance of the low thermal conductivity of air in the cement matrix-air

**Table 8** Gas permeability of the studied composite material

Material	Gas permeability ( $\text{m}^2$ )
K-ref	$3.4 \times 10^{-17}$
K-600	$1.0 \times 10^{-16}$
K-800	$1.6 \times 10^{-16}$
K-1000	$1.9 \times 10^{-16}$

**Table 9** Thermal properties of the studied composite material as a function of moisture content

Material	$w$ (%kg/kg)	$\lambda$ ( $\text{W} \cdot \text{m}^{-1} \cdot \text{K}^{-1}$ )	$c$ ( $\text{J} \cdot \text{kg}^{-1} \cdot \text{K}^{-1}$ )
K-ref	0.0	1.05	830
K-ref	6.0	1.41	820
K-ref	7.0	1.48	910
K-ref	7.2	1.58	890
K-600	0.0	0.76	810
K-600	15.4	1.41	850
K-600	15.7	1.54	910
K-600	16.4	1.66	1030
K-800	0.0	0.66	820
K-800	11.5	1.07	860
K-800	15.7	1.23	870
K-800	18.0	1.64	1070
K-1000	0.0	0.58	820
K-1000	3.6	0.84	800
K-1000	12.7	1.26	1100
K-1000	18.5	1.75	1040

system. The principal loading temperature was again  $600^\circ\text{C}$  where the thermal conductivity decreased by about 30% compared to unloaded specimens. The specific heat capacity of unloaded specimens was almost the same as that of thermally loaded specimens. The differences were within the limits of experimental uncertainty.

The thermal conductivity of the studied fiber reinforced composite increased with increasing moisture content in a very significant way (Table 9). This increase was more remarkable for thermally loaded materials where the thermal conductivity of water-saturated specimens was up to three times higher than in the dry state. For the reference material the thermal conductivity in the water-saturated state was only 50% higher than in the dry state.

The changes in the specific heat capacity due to the changes of moisture content (Table 9) were less important; the maximum differences between the dry state and water-saturated state were only 30%. This is in basic accordance with the general considerations of the theory of mixtures, taking into account the measurement uncertainty.

Figure 8 shows that the PVA fibers exhibited a positive effect on the linear thermal expansion coefficient  $\alpha$  of the studied composite material up to approximately

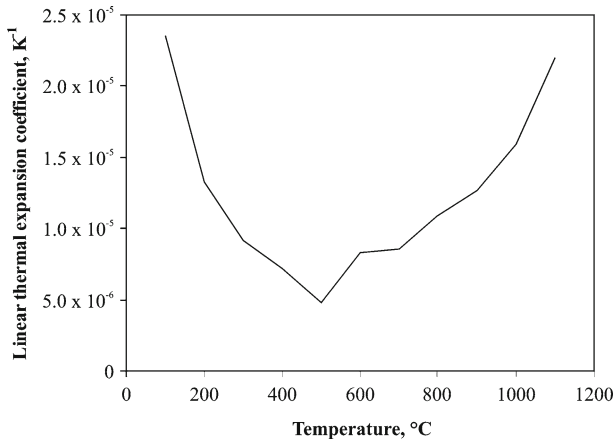


**Fig. 8** Linear thermal expansion coefficient of the studied composite material

500 °C which was even more than could be expected (PVA fibers are supposed to melt at 230 °C to 250 °C);  $\alpha$  decreased four times in that temperature range. For higher temperatures  $\alpha$  began to increase again so that at 1000 °C, it was similar as at room temperature.

Comparing the changes in material properties of the studied hybrid fiber reinforced cement composite induced by thermal pre-treatment with the changes of microstructure caused by thermal decomposition processes at high temperatures, we can see that the changes in the water vapor diffusion resistance factor, gas permeability, and thermal conductivity in the dry state were in reasonable agreement with the deterioration of the material's microstructure. The best indicators of structural damage were tensile and bending strengths which achieved the best agreement with the microstructural analysis and pore size distribution curves over the whole studied temperature range.

In a comparison of the studied hybrid PVA-fiber reinforced composite material with similar materials without fibers investigated in [13–18], the strength decrease with increasing loading temperature was for the fiber-reinforced material in all cases significantly slower. A comparison of the properties of the pore space of the material studied in this paper with cement mortar without fiber reinforcement analyzed in [19] showed that after heating to 800 °C the relative increase of pore volume was for both materials similar but the pore size distribution was different. For cement mortar, the increase of the number of larger pores in the range of 1  $\mu\text{m}$  to 10  $\mu\text{m}$  induced by high-temperature exposure was several times higher than for the hybrid PVA-fiber reinforced composite. These are apparent consequences of the positive effect of PVA fibers which after their melting and subsequent evaporation formed open channels in the cement matrix and prevented it from excessive damage.

## 5 Conclusions

The measurements of mechanical, hygric, and thermal properties of hybrid PVA-fiber reinforced cement composite material after high-temperature exposure presented in

this study have shown that for most parameters, the most important changes occurred between the reference state and the pre-heating temperature of 600 °C where the porosity remarkably increased, the tensile and bending strengths decreased, water vapor transport was greatly accelerated, and heat transport in the dry state was slowed down. The microstructural analysis revealed that the main reason for the observed changes was the thermal decomposition of portlandite and C–S–H gels. Further deterioration of the microstructure at higher temperatures led to the appearance of calcium-silicate minerals, CaO, and SiO<sub>2</sub>. In the reference specimens not subjected to any thermal pre-treatment, the contact between the cement matrix and the PVA fibers was very tight all along the fiber which resulted in satisfactory performance of the composite. The positive effect of using PVA fibers for the high-temperature behavior of the studied composite consisted mainly in their early disintegration which prevented the matrix from explosive spalling.

**Acknowledgment** This research has been supported by the Ministry of Education, Youth and Sports of the Czech Republic, under Project No. MSM: 6840770031.

## References

1. A. Bentur, S. Mindess, *Fibre Reinforced Cementitious Composites* (Elsevier, London, 1990)
2. C.X. Qian, P. Stroeven, *Cem. Concr. Res.* **30**, 63 (2000)
3. W. Sun, H. Chen, X. Luo, H. Qian, *Cem. Concr. Res.* **31**, 595 (2001)
4. S.F.U. Ahmed, M. Maalej, P. Paramasivam, *Constr. Build. Mater.* **21**, 1088 (2007)
5. M. Sahmaran, I.O. Yaman, *Constr. Build. Mater.* **21**, 150 (2007)
6. A. Sivakumar, M. Santhanam, *Cem. Concr. Compos.* **29**, 603 (2007)
7. B. Chen, J. Liu, *Cem. Concr. Res.* **34**, 1065 (2004)
8. G.F. Peng, W.W. Yang, H. Zhao, Y.F. Liu, S.H. Bian, L.H. Zhao, *Cem. Concr. Res.* **36**, 723 (2006)
9. S.L. Suhaendi, T. Horiguchi, *Cem. Concr. Res.* **36**, 1672 (2006)
10. S. Roels, J. Carmeliet, H. Hens, O. Adan, H. Brocken, R. Černý, Z. Pavlík, C. Hall, K. Kumaran, L. Pel, R. Plagge, *J. Therm. Envel. Build. Sci.* **27**, 307 (2004)
11. J. Toman, P. Koudelová, R. Černý, *High Temp. High Press.* **31**, 595 (1999)
12. R. Černý, P. Rovnaníková, *Transport Processes in Concrete* (Spon, London, 2002)
13. Y.N. Chan, G.F. Peng, M. Anson, *Cem. Concr. Compos.* **21**, 23 (1999)
14. C.C. Poon, S. Azhar, M. Anson, Y.L. Wong, *Cem. Concr. Compos.* **25**, 83 (2003)
15. A. Savva, P. Manita, K.K. Sideris, *Cem. Concr. Compos.* **27**, 239 (2005)
16. K.M.A. Hussain, *Cem. Concr. Compos.* **28**, 535 (2006)
17. A. Behnood, H. Ziari, *Cem. Concr. Compos.* **30**, 106 (2008)
18. W.C. Jau, K.L. Huang, *Cem. Concr. Compos.* **30**, 622 (2008)
19. R. Černý, in *Dni betonu*, ed. by P. Kijowski, J. Deja (SPC, Cracow, 2008), p. 329